Analytical and Bioanalytical Chemistry
https://doi.org/10.1007/s00216-020-02449-3

RESEARCH PAPER

Biomembrane-based organic electronic devices for ligand–receptor binding studies

Han-Yuan Liu[1] · Anna-Maria Pappa[2] · Tania Cecilia Hidalgo[3] · Sahika Inal[3] · Róisín M. Owens[2] · Susan Daniel[1]

Received: 2 December 2019 / Revised: 16 January 2020 / Accepted: 22 January 2020

Abstract

We present a simple, rapid method for forming supported lipid bilayers on organic electronic devices composed of conducting polymer electrodes using a solvent-assisted lipid bilayer formation method. These supported bilayers present protein recognition elements that are mobile, critical for multivalent binding interactions. Because these polymers are transparent and conducting, we demonstrate, by optical and electrical detection, the specific interactions of proteins with these biomembrane-based bioelectronic devices. This work paves the way for easy formation of biomembrane mimetics for sensing and detection of binding events in a label-free manner on organic electronic devices of more sophisticated architectures.

Keywords Supported lipid bilayer · PEDOT:PSS · Bioelectronic · Protein recognition · Biosensor

Introduction

The lipid bilayer is the essential structure of the cell membrane and functions as a barrier between the cell interior and its external environment. Beyond barrier function, it plays critical roles in a variety of cellular functions involving complex receptor–ligand engagements important for intracellular signaling [1], cellular recognition [2], and pathogen–host interaction [3]. Supported lipid bilayers (SLBs) have emerged as a useful in vitro platform for studying these receptor–ligand interactions, because they preserve the lateral fluidity of the constituents, while being highly compatible with fluorescence microscopy, a common way to assess these interactions. Lateral fluidity is a key property of SLBs that enables shuffling of the receptors, as in in vivo, to recapitulate multivalent ligand–receptor binding [4], but in a cell-free platform.

SLBs can be formed via several techniques including Langmuir–Blodgett (LB) and Langmuir–Schaefer (LS) deposition [5], solvent-assisted lipid bilayer (SALB) formation [6, 7], or vesicle fusion (VF) [8]. Each technique has advantages and disadvantages. The latter two enable self-assembly of the lipid bilayer in situ, which is compatible with microfluidic devices and enables a direct path toward massively parallel and highly quantitative systems for screening of biological compounds [9]. For example, a "one-shot" binding curve can be readily obtained using parallel supported bilayer-coated microfluidic channels in a device that, when combined with fluorescence microscopy, can provide data to quickly access the binding strength of a particular ligand–receptor combination [10, 11].

While such advances provide important information in protein recognition studies [4, 12, 13], there remain challenges for detection. Although fluorescently protein labeling is by far the most frequently used strategy for identifying positive receptor–ligand interactions, the process of labeling can be difficult and laborious. Moreover, labels have the potential to inactivate the biomolecule of interest or perturb its capacity to interact as it would in a nonlabeled state [14]. Label-free detection methods, such as surface plasmon resonance (SPR) [15], quartz crystal microbalance (QCM) [16], surface-

Published in the topical collection featuring *Female Role Models in Analytical Chemistry.*

Electronic supplementary material The online version of this article (https://doi.org/10.1007/s00216-020-02449-3) contains supplementary material, which is available to authorized users.

✉ Susan Daniel
SD386@cornell.edu

[1] Robert F. Smith School of Chemical and Biomolecular Engineering, Cornell University, Ithaca, NY 14853, USA

[2] Department of Chemical Engineering and Biotechnology, University of Cambridge, Cambridge CB3 0AS, UK

[3] Biological and Environmental Science and Engineering Division, King Abdullah University of Science and Technology (KAUST), Thuwal 23955-6900, Saudi Arabia

Published online: 05 February 2020

enhanced Raman scattering (SERS) [17], and microcantilevers [18], utilize molecular biophysical properties and various transducing mechanisms offering alternative ways to study ligand–receptor interactions and protein recognition events. However, multi-modal detection has the benefit of increasing confidence in measurements. One class of materials that can meet this dual modality readout is conducting polymers.

Conducting polymer devices can be fabricated into transparent, thin films, maintaining compatibility with optical/fluorescent tracking features. Conducting polymer devices have been utilized extensively for label-free transduction of changes in local ionic and/or electrical properties [19–21]. Furthermore, the mechanical properties of conducting polymers can be matched with biotic tissue [22, 23], providing a biocompatible interface to the bilayer that is more realistic than the hard oxide surfaces typically used as supports for SLBs. These materials are thus of great interest for integration with SLBs for optical and electrical transduction for sensing applications.

One conducting polymer in particular, poly(3,4-ethylenedioxythiophene) polystyrene sulfonate (PEDOT:PSS), has emerged as one of the most promising organic electronic materials because of its high conductivity, optical transparency, excellent stability, and easy processing [24]. We have already demonstrated the ability to interface lipid bilayers with PEDOT:PSS thin films and devices via the VF method [25]. However, this method had limited compatibility with this surface: only vesicles composed of lipids from Archaea were able to rupture to form SLB patches on the PEDOT:PSS films. In later work [26], we circumvented this limitation by changing to another method of bilayer self-assembly: the SALB formation. SALB exploits the phase transition of lipid structures from adsorbed micelles to a planar bilayer structure when a solvent is slowly exchanged for aqueous buffer in a microfluidic device [6, 7]. The lipid molecules first absorb onto the surface in the presence of an organic solvent, such as methanol, ethanol, or isopropanol. Then, sequential solvent exchange that introduces an aqueous buffer promotes the self-assembly of SLB on the surface as the water content is slowly increased. [6] Using SALB to bypass vesicle preparation and the subsequent strict requirements for their rupture to form an SLB really expands the types of bilayers that can be formed, including challenging ones such as the highly negatively charged bacterial membrane mimics [26]. In this work, we leverage the SALB method to form a SLB made from phospholipids and biotinylated lipids (used herein as the protein recognition elements) supported on PEDOT:PSS films to demonstrate the utility of the platform for sensing ligand–receptor binding using both optical and electrical means (Fig. 1a). First, we form and characterize the membrane fluidity of the SLB on the conducting polymer. Then, we characterize the binding between a fluorescent-labeled streptavidin and the biotinylated lipids via fluorescence microscopy. Next, we demonstrate electrical sensing of binding events using electrochemical impedance spectroscopy (EIS) (Fig. 1b). These results open the door for future work where both sensing modes can be used simultaneously for protein recognition in biosensing, or membrane biophysical studies on more complicated device architectures.

Materials and methods

Preparation of lipid mixtures

Two lipid compositions were used in this work: 100% (mol/mol) and 97% (mol/mol) 1,2-dioleoyl-*sn*-glycero-3-phosphocholine (DOPC) and 3% (mol/mol) 1,2-dioleoyl-*sn*-glycero-3-phosphoethanolamine-*N*-(cap biotinyl) (biotin-cap-DOPE). DOPC and biotin-cap-DOPE were purchased from Avanti Polar Lipids (Alabaster, AL).

For the SALB method, lipid mixtures were prepared by mixing lipids in chloroform in the desired ratio. Chloroform was gently evaporated under a stream of nitrogen. Then, the lipid films were stored under vacuum for 3 h to remove any residual chloroform. Then, isopropanol (VWR) was added to a concentration of 1 mg/mL to create a solution of lipids in solvent that was used as described below to form the bilayers.

PEDOT:PSS solution preparation

The solution mixture composed of 95% v/v Clevios™ PH 1000 (Heraeus), 5% v/v ethylene glycol (Sigma-Aldrich), 0.002% v/v 4-dodecylbenzenesulfonic acid (Sigma-Aldrich), and 1% v/v (3-glycidyloxypropyl)trimethoxysilane (Sigma-Aldrich) was sonicated (Ultrasonic Cleaner, VWR) for 30 min and flowed through a 0.45-μm filter (EZFlow Syringe Filter, Thomas Scientific) prior to use.

Surface support preparation

Glass slides were cleaned by piranha solution (70% (v/v) H_2SO_4 (BDH) and 30% (v/v) H_2O_2 (Sigma, 50 wt%)) for 10 min and rinsed by flushing DI water for 20 min continuously. The glass slides were then treated with oxygen plasma (Harrick Plasma, Ithaca, NY) at a pressure of 750 mTorr with power of 18 W for 2 min. To prepare PEDOT:PSS films on these surfaces, glass slides were spin-coated (Apogee Spin Coater, Cost Effective Equipment) with the PEDOT:PSS solution at 2500 rpm for 35 s, followed by annealing at 140 °C for 1 h. Coated PEDOT:PSS surfaces were immersed into DI water for 4 h and treated with oxygen plasma for 2 min before use.

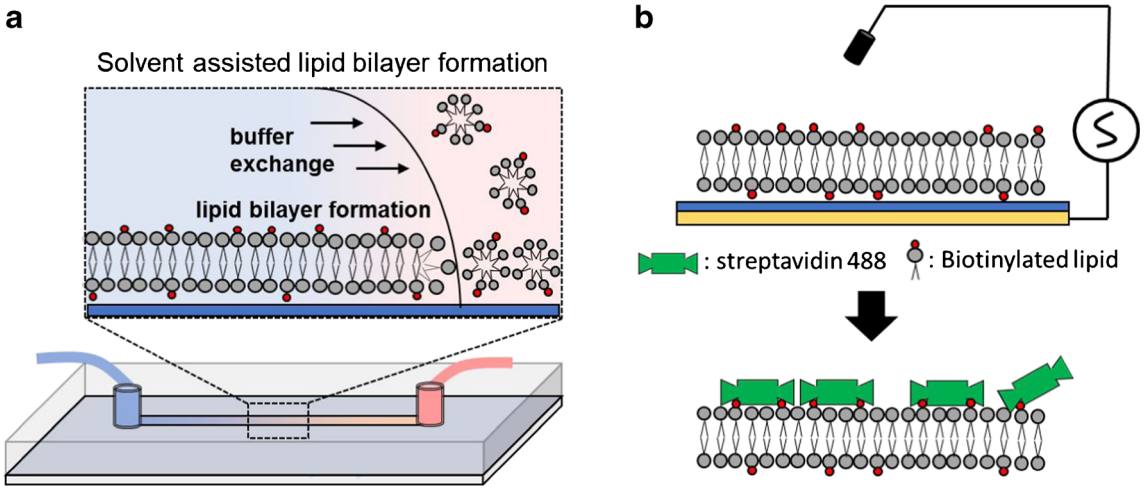

Fig. 1 (**a**) The solvent-assisted lipid bilayer (SALB) formation occurs after lipid micelles adsorb onto the PEDOT:PSS film (dark blue) and convert into a continuous lipid planar bilayer during the solvent (pink) exchange with aqueous buffer (light blue) process. (**b**) Electrochemical impedance spectroscopy measurements on PEDOT:PSS electrodes formed on gold are used to sense the protein–ligand interaction between streptavidin (green features) and biotin (red dots) via the supported lipid bilayer with incorporated biotinylated lipids

Lipid bilayer formation

In this work, the microfluidic channel attached on either plain glass slides or PEDOT:PSS surfaces was provided by the Engineering in Translational Science Group at Nanyang Technical University. The microfluidic channel used in this study is comprised of a straight channel with two ports which serve as the inlet and outlet for solutions. For the SALB formation method, the lipid solution in solvent was delivered into the microfluidic channel at a flow rate of 100 μl/min and static incubated for 30 min. After incubation, Tris buffer was drawn into microfluidic channel at a flow rate of 50 μl/min to remove excess lipids and induce formation of the lipid bilayer on the glass surface or PEDOT:PSS film.

Fluorescence recovery after photobleaching on characterization of bilayers

After bilayers are formed on glass or PEDOT:PSS surfaces, fluorescence recovery after photobleaching (FRAP) was carried out with an inverted Zeiss Axio Observer.Z1 microscope with α Plan-Apochromat × 20 objectives to determine the fluidity of the SLB. With all lipid compositions, 0.5% (mol/mol) Texas Red 1,2-dihexadecanoyl-*sn*-glycero-3-phosphoethanolamine (TR-DHPE) was used as a fluorescent probe. A 20-μm-diameter spot in bilayer was bleached by a 150-mW, 561-nm optically pumped semiconductor laser (Coherent, Inc.) for 500 ms. The recovery of the bleached spot was monitored for 30 min, and the fluorescence intensity of the spot was determined and normalized in each image. The data of fluorescence intensity was fit with a Bessel function following the method of Soumpasis [27]. To obtain the diffusion coefficient (D), the following equation was used: $D = w^2/4t_{1/2}$, where w is the radius of the photobleached spot at half maximum and $t_{1/2}$ is the time required to achieve half of the maximum recovery intensity. Mobile fraction is defined as the ratio of the recovered spot fluorescence intensity over the initial fluorescence intensity in the same area.

Fluorescence microscopy imaging of biomolecule binding

Alexa Fluor 488 streptavidin was purchased from Thermo Fisher. Two hundred nanomolars of Alexa Fluor 488 streptavidin in Tris buffer was delivered into the microfluidic channel at a flow rate of 100 μl/min and incubated for 10 min. Then, the Tris buffer was drawn into the channel to remove unbound protein at a flow rate of 100 μl/min with continuous flow for 1 min. Images were recorded by an inverted Zeiss Axio Observer.Z1 microscope equipped with α Plan-Apochromat × 20 objective, X-Cite 120 microscope light source (Lumen Dynamics Group, Inc.), and AxioCam MRm camera (Zeiss) at the exposure time of 400 ms.

Electrode fabrication

All electrodes were fabricated using standard photolithographic techniques. Glass substrates were cleaned in hot piranha bath and later exposed to an oxygen plasma to ensure complete removal of contaminants. Electrode patterns were transferred to the substrates using a bilayer resist structure (LOR 5B, Microchem; S1813, Shipley); 10 nm of Cr and 100 nm of Au were deposited via magnetron sputtering to realize the electrodes (ESCRD4, Equipment Support Company, Ltd.). An encapsulation layer of parylene C was deposited to insulate gold interconnects via vaporization (SCS Labcoter 2), which was adhered to the substrates using 3-(trimethoxysilyl)propyl methacrylate. A sacrificial second

layer of parylene C was deposited for polymer patterning. A thick positive photoresist (AZ9260, Microchemicals) was used to pattern electrode and contact pad areas, which was later removed by O_2 plasma (Oxford Instruments Plasmalab 100 ICP-380).

Electrochemical impedance spectroscopy measurement for lipid bilayer formation and detection of biomolecule binding

Ag/AgCl electrode was used as reference electrode, and a platinum mesh (45 mm × 25 mm) was used as counter electrode. The working PEDOT:PSS electrode had a round shape and a radius of 500 μm. Impedance spectra of the PEDOT:PSS/SLB platform were measured using an Autolab potentiostat (PGSTAT302) equipped with a frequency response analysis module. The AC voltage of 0.01 V and the DC voltage of 0 mV versus open-circuit potential were applied. The electrolyte solution was Tris buffer, unless otherwise stated. The measured data were fit to a model represented by equivalent circuits composed of an electrolyte resistance and two RC elements in series which represent the SLB and PEDOT:PSS electrode, respectively.

Results and discussion

Formation of biotinylated SLB on glass and PEDOT:PSS

We first show the formation of SLBs via the SALB method on PEDOT:PSS films spin-coated on glass. Given that the PEDOT:PSS film is transparent, both surfaces, glass and PEDOT:PSS, are compatible with optical microscopy. Therefore, incorporating fluorescent-labeled lipids into the lipid mixture allowed us to assess the bilayer formation as well as characterize their two-dimensional diffusivity using FRAP. As shown in Fig. 2 a and b, the biotinylated SLB successfully formed on both plain glass and PEDOT:PSS surfaces using the SALB method, and both preserved the membrane fluidity (the photobleached spot fully recovered after 5 min in both cases).

To quantitatively analyze the membrane fluidity, the recovery of fluorescence intensity with time was used to calculate the diffusion coefficient (D) and determine the mobile fraction (MF) (Fig. 2c, d). The diffusion coefficient and mobile fraction of biotinylated SLB on glass slides and PEDOT:PSS are as follows: $D = 1.27 \pm 0.032$ μm^2/s and MF = 1.00 ± 0.006 and $D = 0.54 \pm 0.101$ μm^2/s and MF = 0.98 ± 0.032, respectively. The results of biotinylated SLBs formed via SALB on glass slides are aligned with previous literature reported by us [26] and others [28, 29]. However, on PEDOT:PSS, even though the MF is near 100%, we observed a significant decrease in the D value of the SLB formed on the PEDOT:PSS surface, relative to the glass counterpart. The high MF suggests that the quality of the bilayer is very good, with minimal unruptured micelles or discontinuous patches. However, the diffusion coefficient is about half the value on glass. Some possible reasons for the reduced D value are that, unlike inorganic silica-based surfaces that are relatively smooth, the surface of PEDOT:PSS is relatively rough. The roughness of the glass slides after treatment of piranha wash has been reported to be around 0.1–0.2 nm [30]. The roughness of PEDOT:PSS films, which are about 0.47 nm, is slightly higher than the glass surface. The polymer thin film swells in aqueous solution which further increases roughness [31]. The roughness of PEDOT:PSS films in aqueous solution has been shown as about 1.5 nm which is 6–7-fold higher than the glass surface [31]. In a previous study, Blachon et al. [32] reported the impact of nanoroughness on membrane fluidity and showed that with increasing roughness, the decrease in diffusion coefficient can result from either defects or increased surface area over which the bilayer conforms. Our case appears to be more aligned with having increased surface area. However, we note that the surface of PEDOT:PSS can promote some pinning of zwitterionic lipids onto the polymer momentarily that could lead to a reduced diffusion coefficient as well. We have not explored the cause of this reduction in our system and note that the main point here is that the bilayer has mobility and thus should be able to rearrange as needed to make multivalent contacts during protein binding.

Validation of protein–ligand binding via fluorescence microscopy

After characterization of SLB formation and its fluidity, we next investigated protein–ligand binding between Alexa Fluor 488–conjugated streptavidin and the biotinylated lipids in the SLB using fluorescence microscopy. To determine if nonspecific binding of streptavidin occurs, we first examined the streptavidin interaction with a bare PEDOT:PSS surface as well as with a pure DOPC bilayer (no biotin) on PEDOT:PSS. As shown in Fig. 3 a, images of the PEDOT:PSS surface indicate little nonspecific binding of Alexa Fluor 488–conjugated streptavidin to the PEDOT:PSS surface. This is reasonable because the electrostatic repulsion between the negatively charged Alexa Fluor 488–conjugated streptavidin and negatively charged PEDOT:PSS inhibits binding. Similarly, as shown in Fig. 3 b, streptavidin does not bind to the pure DOPC bilayer either. Next, we examined the specific protein recognition of streptavidin to the biotinylated SLBs. As shown in Fig. 3 c, the fluorescence microscopy images indicate a significant amount of streptavidin binding due to the presence of the biotin ligand present in the SLB. This measurement was repeated with a range of streptavidin concentrations. Figure 3 d summarizes the fluorescence

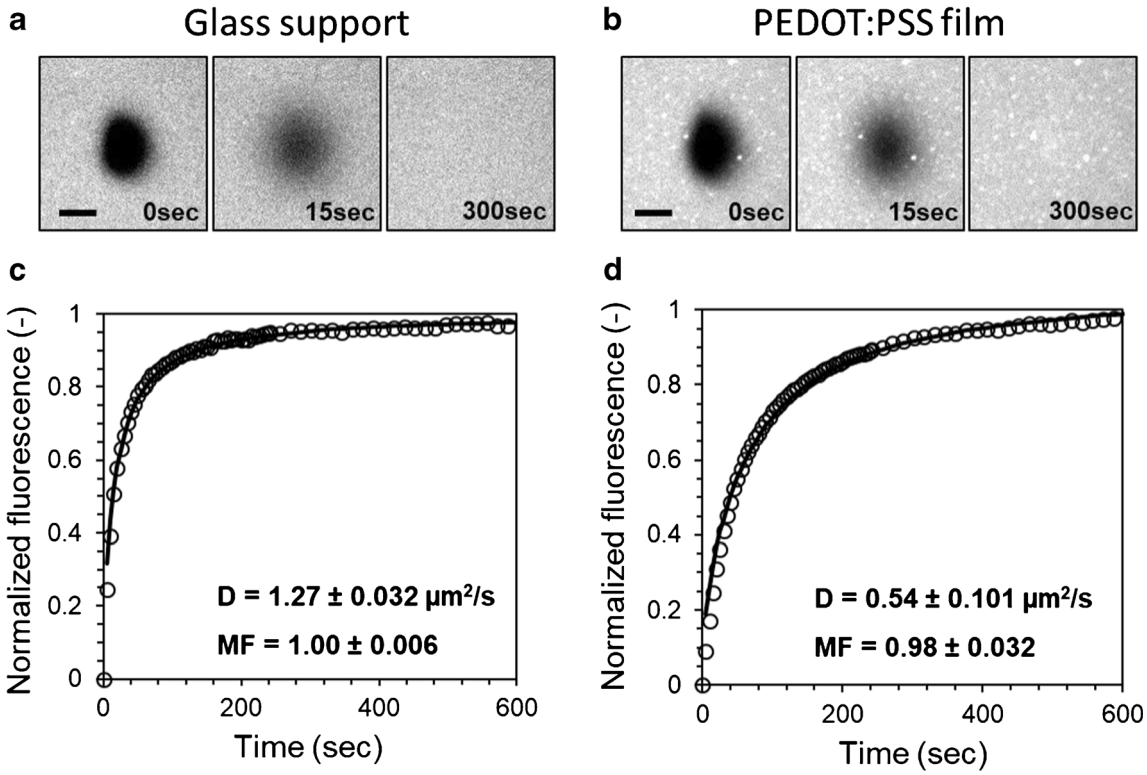

Fig. 2 Microscopy images of fluorescence recovery after photobleaching (FRAP). The photobleached spots in bilayers formed by the SALB method fully recover on (**a**) glass and (**b**) PEDOT:PSS surfaces. The recovery of fluorescence intensity with time for biotinylated SLB on (**c**) glass and (**d**) PEDOT:PSS surface is used to calculate the diffusion coefficient (*D*) of lipids in each SLB and the mobile fraction. The scale bar is 20 μm

intensity levels of all the aforementioned samples and controls, with the 200 nM streptavidin showing the maximum intensity with a ~6-fold increase compared to the baseline. Taken altogether, our results confirm the successful incorporation of biotin as recognition elements (via the use of biotinylated lipids) into an SLB formed on PEDOT:PSS films by the SALB method and the ability of this platform to be sensitive and specific for sensing streptavidin using optical methods.

Characterization of protein–ligand binding to SLB on the PEDOT:PSS electrode via EIS

After using conventional optical-based assays to characterize specific protein binding on the biotinylated biomembrane, we next take advantage of the conductivity of the PEDOT:PSS surface and perform electrical measurements. We employed EIS to investigate the capability of our platform to sense protein binding. The biotinylated SLB was first characterized with no streptavidin present as baseline. Then, the biotinylated SLB was incubated with streptavidin at various concentrations ranging from 0 to 200 nM. As shown in Fig. 4 a, streptavidin specifically binds to the SLB containing biotin. The impedance spectra indicate a significant increase in the impedance value in the mid-range frequencies (10–1000 Hz) as the concentration of streptavidin increases, mirroring what was observed optically over this concentration range. As shown in Fig. 4 b, contrary to the impedance changes observed after streptavidin addition in the biotinylated biomembrane, the control experiment adding bovine serum albumin (BSA) showed no change in the impedance spectra with an increasing concentration of BSA from 0 to 200 nM. These results confirm that the change in signal observed with streptavidin is indeed due to the specific interaction between the biotinylated bilayer and streptavidin.

SLBs and the interactions occurring at the membrane surface on electrodes typically lead to significant changes in impedance, particularly in mid-range frequencies, between 10^1 and 10^4 Hz [33]. The mid-range frequencies are most sensitive for sensing at the membrane surface in this architecture. At very high frequencies, the sensitivity is not high because the frequency change is such that the ionic response can only be observed within the electrolyte where fast rearrangements can occur. At very low frequencies, the signal approaches a DC signal and monitors very slow timescale changes. In the intermediate frequency range, we are sensitive to the membrane because the ionic arrangements are influenced by both the electrolyte and the membrane environment.

To show more clearly the concentration dependence effect on protein binding using EIS, we chose to present the relative

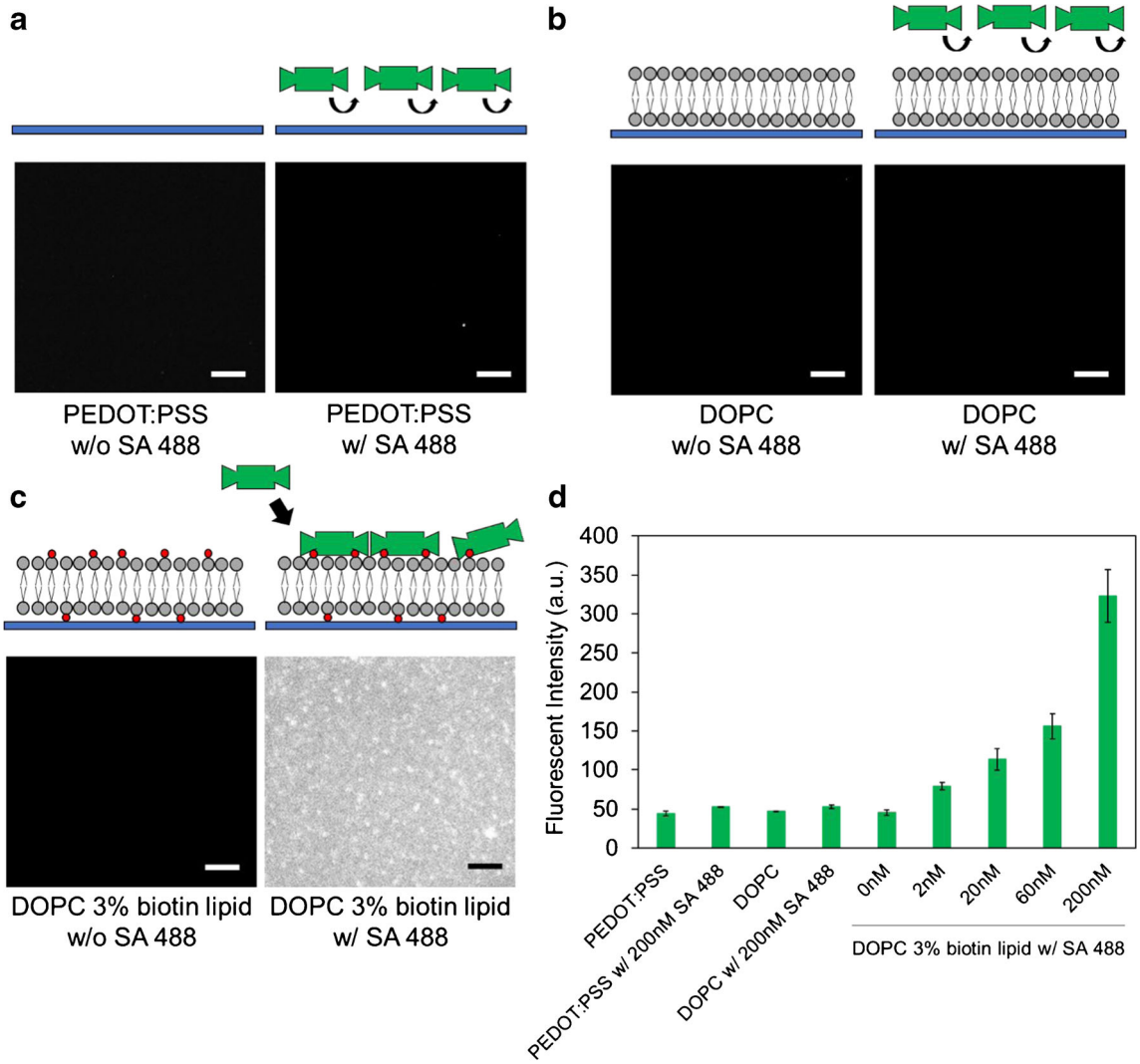

Fig. 3 Validation of the interaction between Alexa Fluor 488–conjugated streptavidin (SA 488) and biotinylated lipid through fluorescence microscopy. (**a**) Microscopic images of the interaction between Alexa Fluor 488–conjugated streptavidin (200 nM) and PEDOT:PSS surface. (**b**) Microscopic images of the interaction between Alexa Fluor 488–conjugated streptavidin (200 nM) and DOPC bilayer. (**c**) Microscopic images of the binding of Alexa Fluor 488–conjugated streptavidin (200 nM) to DOPC 3% biotinylated lipid bilayer. (**d**) The fluorescence intensity of each case (**a**–**c**), as well as the response to various concentrations of protein solution. The scale bar is 20 μm

impedance change at a single frequency where we observe the maximum change in the EIS spectra. As points of comparison, in a previous study, Poltorak et al. [34] demonstrated SLB formation on polyelectrolyte-based films on doped silicon surfaces. Their results show a reproducible increase in impedance in the range of 10^1–10^4 Hz due to the deposition of a lipid bilayer, and they subsequently examined the change in impedance at around 150 Hz, the maximum change in impedance magnitude they observed. Sugihara et al. [35] have shown lipid bilayer formation on ITO surfaces modified with polyethyleneimine (PEI) layers and demonstrated EIS measurements to detect the interaction of pore-forming toxin at the bilayer. They also observed a change in impedance in the range of 10^2–10^3 and examined the impedance change at 750 Hz, which is the maximum change in impedance magnitude they observed. In this work, the maximum change in signal is observed in the 10–1000 Hz range and is most pronounced at 100 Hz. Thus, we chose this frequency to plot the relationship of the impedance changes with protein concentration, as shown in Fig. 5. For the control case (BSA addition), as expected, the relative change of impedance remains near zero over the same concentration range. As streptavidin is added, impedance increases with increasing concentration. Over the range of concentrations tested, the change of impedance after the addition of 2 nM streptavidin is small; however, it increases above the nonspecific control after the addition of 20 nM.

To quantitatively analyze the EIS data, we modeled the data with an equivalent electrical circuit (see Electronic Supplementary Material (ESM) Fig. S1) which is commonly

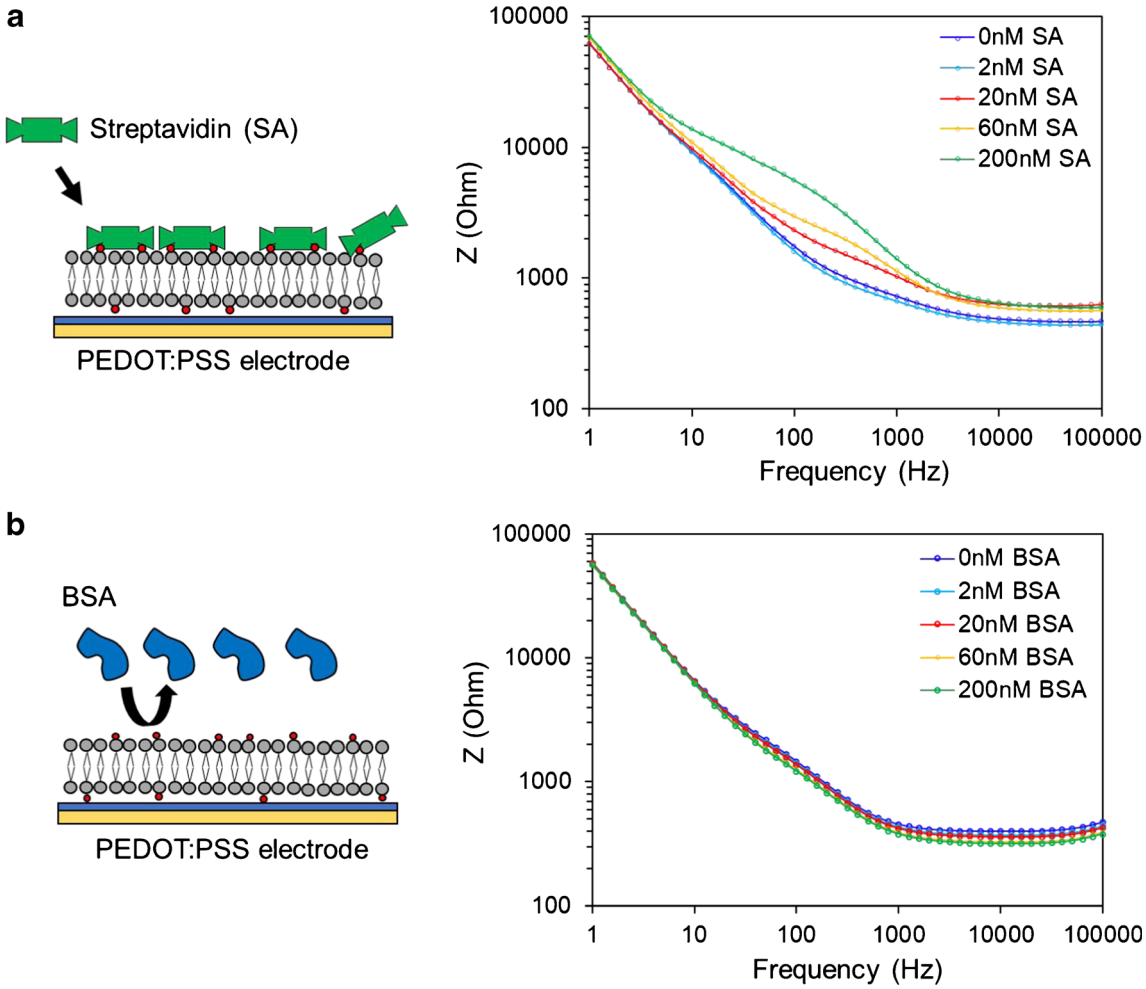

Fig. 4 Characterization of protein–ligand binding through electrochemical impedance spectroscopy. (**a**) Illustration of streptavidin binding to biotinylated SLB and the corresponding Bode plot characterizing the electrical response on the SLB after incubation with streptavidin at various concentrations. (**b**) Illustration of BSA unable to bind to a biotinylated SLB and the corresponding Bode plot for the SLB after incubation with BSA at various concentrations

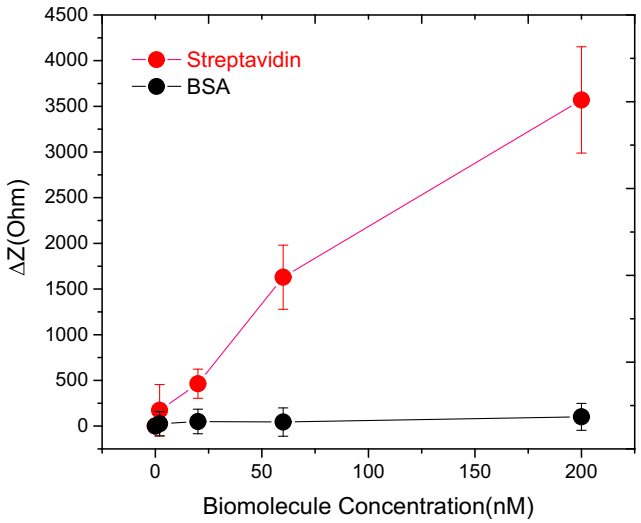

Fig. 5 The change in the magnitude of impedance recorded at 100 Hz as a function of biomolecule concentration. Red symbol: streptavidin; black symbol: BSA

used to interpret the impedance of SLB and its interaction with biomolecules [36]. The model includes the resistance of the electrolyte (R_s), the impedance of the PEDOT:PSS (represented by a resistor (R_p) in parallel with a capacitor (C_p)), and the impedance of the lipid bilayer (a resistor (R_b) in parallel with a capacitor (C_b)) (inset, Fig. 6a).

The calculated resistance and capacitance of SLB are $R_b = 4.09 \pm 0.83$ kΩ/cm^2 and $C_b = 418.46 \pm 31.70$ μF/cm^2, respectively. As the concentration of streptavidin increases, the model estimates an increase in R_b and a decrease in C_b (Fig. 6a, b). As shown in Fig. 6 a, the change of resistance (ΔR_b) is about 60% at 200 nM streptavidin. The increase of resistance is attributed to protein recognition leading to more mass adsorption at SLB and altering its electrical property [37]. Figure 6 b shows the change of capacitance (ΔC_b) is about − 20% at 200 nM streptavidin. This could be attributed to streptavidin binding causing an increase in the distance between the electrolyte and electrode surface [38]. In Fig. 6 c, the bound protein introduces a new capacitive component at higher

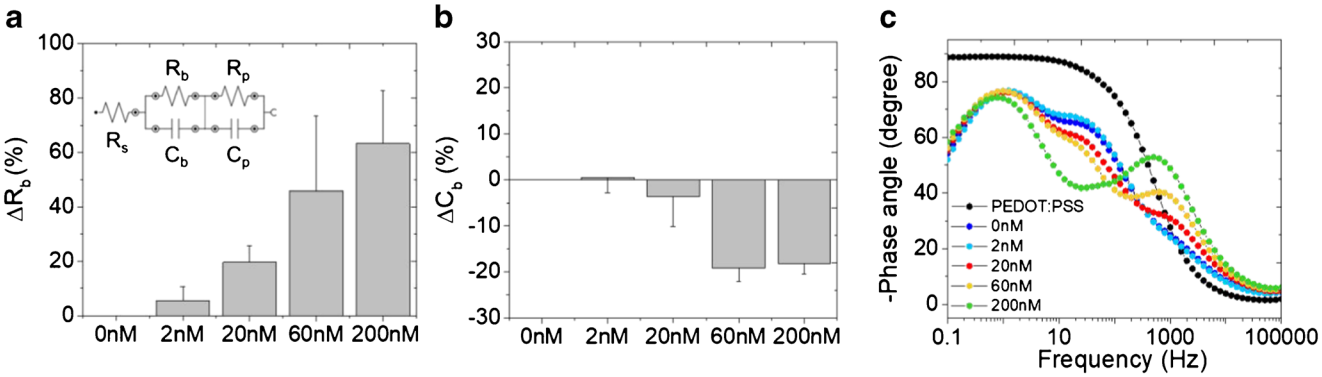

Fig. 6 (**a**) The effect of streptavidin binding on resistance at increasing concentration. Inset shows the equivalent electrical circuit for modeling electrical parameters of the system. (**b**) The effect of streptavidin binding on capacitance of SLB at increasing concentration. (**c**) The phase plot of impedance measurements

frequencies, as a peak emerges in the phase diagram as concentration increases. Examining the Nyquist plots as well, the formation of new component in the circuit is apparent from the shift of the shape of the curves as concentration increases (ESM Fig. S2). These changes can be modeled as a third capacitor in series with the bilayer. In this case, the total capacitance will decrease with the increase of binding events, following the working principle of capacitive immunosensors [39]. As such, the total capacitance of the system becomes frequency dependent, as we observed here.

Conclusions

In this work, we demonstrate the formation of a solvent-assisted lipid bilayer containing a ligand for protein recognition on the surface of a conducting polymer made of PEDOT:PSS. Because of the planar geometry, transparency, and the conductivity and biocompatibility of PEDOT:PSS with a lipid bilayer, this platform permits quantitative biosensing of complex biomolecule interactions via optical or electrical measurements. We demonstrate specific protein recognition via both fluorescence microscopy and electrochemical impedance spectroscopy. Taken together, the results indicate the SALB formation method is a promising approach for rapidly fabricating SLBs that present cell membrane–like surfaces that have mobile functional groups on conducting polymer surfaces. In the application of protein binding, mobility is critical to ensure it is possible to make multivalent interactions as is often exploited by nature to increase binding strength to the membrane. It is possible in the future for this bilayer formation strategy and detection scheme to be adapted to more advanced organic electronic device architectures, such as transistors, which can allow the *simultaneous* optical and electrical detection of binding events. Such devices will expand the sensitivity of the platform, paving the way for next-generation biosensors that preserve key features in an all-in-one platform of membrane fluidity, ligand presentation, simultaneous dual sensing capability, and compatibility with microfluidics for high-throughput sensing and screening.

Acknowledgments We thank Professor Nam-Joon Cho (the Engineering in Translational Science Group at Nanyang Technical University) for his advice and providing the microfluidic flow cells used in this work. The views and conclusions contained in this document are those of the authors and should not be interpreted as representing the official policies, either expressed or implied, of DARPA or the Army Research Office or the U.S. Government.

Funding information A.M.P. received funding from the Oppenheimer Junior Research Fellowship. Part of this work was supported by the King Abdullah University of Science and Technology (KAUST) Office of Sponsored Research (OSR) under Award No. OSR-2018-CRG7-3709. This research was sponsored in part by the Defense Advanced Research Projects Agency (DARPA) Army Research Office and was accomplished under Cooperative agreement number W911NF-18-2-0152.

Compliance with ethical standards

Conflict of interest The authors declare that they have no conflict of interest.

References

1. Dijkman PM, Watts A. Lipid modulation of early G protein-coupled receptor signalling events. Biochim Biophys Acta Biomembr. 2015;1848(11):2889–97.
2. Qi S, Groves JT, Chakraborty AK. Synaptic pattern formation during cellular recognition. Proc Natl Acad Sci U S A. 2001;98(12):6548–53.
3. Yang S-T, Kiessling V, Simmons JA, White JM, Tamm LK. HIV gp41–mediated membrane fusion occurs at edges of cholesterol-rich lipid domains. Nat Chem Biol. 2015;11(6):424.
4. Jung H, Robison AD, Cremer PS. Multivalent ligand–receptor binding on supported lipid bilayers. J Struct Biol. 2009;168(1):90–4.
5. Liu J, Conboy JC. Structure of a gel phase lipid bilayer prepared by the Langmuir−Blodgett/Langmuir-Schaefer method characterized by sum-frequency vibrational spectroscopy. Langmuir. 2005;21(20):9091–7.

6. Ferhan AR, Yoon BK, Park S, Sut TN, Chin H, Park JH, et al. Solvent-assisted preparation of supported lipid bilayers. Nat Protoc. 2019;1.
7. Hohner AO, David MPC, Rädler JO. Controlled solvent-exchange deposition of phospholipid membranes onto solid surfaces. Biointerphases. 2010;5(1):1–8.
8. Richter RP, Bérat R, Brisson AR. Formation of solid-supported lipid bilayers: an integrated view. Langmuir. 2006;22(8):3497–505.
9. Sia SK, Whitesides GM. Microfluidic devices fabricated in poly (dimethylsiloxane) for biological studies. Electrophoresis. 2003;24(21):3563–76.
10. Albertorio F, Daniel S, Cremer PS. Supported lipopolymer membranes as nanoscale filters: simultaneous protein recognition and size-selection assays. J Am Chem Soc. 2006;128(22):7168–9.
11. Yang T, S-y J, Mao H, Cremer PS. Fabrication of phospholipid bilayer-coated microchannels for on-chip immunoassays. Anal Chem. 2001;73(2):165–9.
12. Shi J, Yang T, Kataoka S, Zhang Y, Diaz AJ, Cremer PS. GM1 clustering inhibits cholera toxin binding in supported phospholipid membranes. J Am Chem Soc. 2007;129(18):5954–61.
13. Salaita K, Nair PM, Petit RS, Neve RM, Das D, Gray JW, et al. Restriction of receptor movement alters cellular response: physical force sensing by EphA2. Science. 2010;327(5971):1380–5.
14. Toseland CP. Fluorescent labeling and modification of proteins. J Chem Biol. 2013;6(3):85–95.
15. Campbell CT, Kim G. SPR microscopy and its applications to high-throughput analyses of biomolecular binding events and their kinetics. Biomaterials. 2007;28(15):2380–92.
16. Cho N-J, Frank CW, Kasemo B, Höök F. Quartz crystal microbalance with dissipation monitoring of supported lipid bilayers on various substrates. Nat Protoc. 2010;5(6):1096.
17. Campion A, Kambhampati P. Surface-enhanced Raman scattering. Chem Soc Rev. 1998;27(4):241–50.
18. Wu G, Datar RH, Hansen KM, Thundat T, Cote RJ, Majumdar A. Bioassay of prostate-specific antigen (PSA) using microcantilevers. Nat Biotechnol. 2001;19(9):856.
19. Pappa A-M, Parlak O, Scheiblin G, Mailley P, Salleo A, Owens RM. Organic electronics for point-of-care metabolite monitoring. Trends Biotechnol. 2018;36(1):45–59.
20. Rivnay J, Inal S, Salleo A, Owens RM, Berggren M, Malliaras GG. Organic electrochemical transistors. Nat Rev. 2018;3(2):17086.
21. Pitsalidis C, Pappa A, Moysidou C, Iandolo D, Owens R. Conducting and conjugated polymers for biosensing applications. In: Conjugated polymers: CRC; 2019. p. 697–742.
22. Liu H-Y, Chen W-L, Ober CK, Daniel S. Biologically complex planar cell plasma membranes supported on polyelectrolyte cushions enhance transmembrane protein mobility and retain native orientation. Langmuir. 2017;34(3):1061–72.
23. Tanaka M, Sackmann E. Polymer-supported membranes as models of the cell surface. Nature. 2005;437(7059):656.
24. Strakosas X, Bongo M, Owens RM. The organic electrochemical transistor for biological applications. J Appl Polym Sci. 2015;132(15).
25. Zhang Y, Inal S, Hsia CY, Ferro M, Ferro M, Daniel S, et al. Supported lipid bilayer assembly on PEDOT:PSS films and transistors. Adv Funct Mater. 2016;26(40):7304–13.
26. Su H, Liu H-Y, Pappa A-M, Hidalgo TC, Cavassin P, Inal S, et al. Facile generation of biomimetic-supported lipid bilayers on conducting polymer surfaces for membrane biosensing. ACS Appl Mater Interfaces. 2019;11(47):43799–810.
27. Soumpasis DM. Theoretical analysis of fluorescence photobleaching recovery experiments. Biophys J. 1983;41(1):95–7.
28. Tabaei SR, Choi J-H, Haw Zan G, Zhdanov VP, Cho N-J. Solvent-assisted lipid bilayer formation on silicon dioxide and gold. Langmuir. 2014;30(34):10363–73.
29. Tabaei SR, Jackman JA, Kim S-O, Liedberg B, Knoll W, Parikh AN, et al. Formation of cholesterol-rich supported membranes using solvent-assisted lipid self-assembly. Langmuir. 2014;30(44):13345–52.
30. Seu KJ, Pandey AP, Haque F, Proctor EA, Ribbe AE, Hovis JS. Effect of surface treatment on diffusion and domain formation in supported lipid bilayers. Biophys J. 2007;92(7):2445–50.
31. ElMahmoudy M, Inal S, Charrier A, Uguz I, Malliaras GG, Sanaur S. Tailoring the electrochemical and mechanical properties of PEDOT:PSS films for bioelectronics. Macromol Mater Eng. 2017;302(5):1600497.
32. Blachon F, Harb F, Munteanu B, Piednoir A, Fulcrand R, Charitat T, et al. Nanoroughness strongly impacts lipid mobility in supported membranes. Langmuir. 2017;33(9):2444–53.
33. Atanasov V, Knorr N, Duran RS, Ingebrandt S, Offenhäusser A, Knoll W, et al. Membrane on a chip: a functional tethered lipid bilayer membrane on silicon oxide surfaces. Biophys J. 2005;89(3):1780–8.
34. Poltorak L, Verheijden ML, Bosma D, Jonkheijm P, de Smet LC, Sudhölter EJ. Lipid bilayers cushioned with polyelectrolyte-based films on doped silicon surfaces. Biochim Biophys Acta Biomembr. 2018;1860(12):2669–80.
35. Sugihara K, Delai M, Szendro I, Guillaume-Gentil O, Vörös J, Zambelli T. Simultaneous OWLS and EIS monitoring of supported lipid bilayers with the pore forming peptide melittin. Sens Actuators B Chem. 2012;161(1):600–6.
36. Purrucker O, Hillebrandt H, Adlkofer K, Tanaka M. Deposition of highly resistive lipid bilayer on silicon–silicon dioxide electrode and incorporation of gramicidin studied by ac impedance spectroscopy. Electrochim Acta. 2001;47(5):791–8.
37. Grieshaber D, MacKenzie R, Vörös J, Reimhult E. Electrochemical biosensors-sensor principles and architectures. Sensors. 2008;8(3):1400–58.
38. Ertürk G, Mattiasson B. Capacitive biosensors and molecularly imprinted electrodes. Sensors. 2017;17(2):390.
39. Mattiasson B, Hedström M. Capacitive biosensors for ultrasensitive assays. TrAC Trends Anal Chem. 2016;79:233–8.